OPEN ACCESS
IOP Publishing
Superconductor Science and Technology
Supercond. Sci. Technol. **34** (2021) 085018 (10pp)
https://doi.org/10.1088/1361-6668/ac0951

Improved pulsed field magnetisation in MgB_2 trapped-field magnets

D A Moseley[1,*], G A B Matthews[2], D Zhou[3], V Cientanni[1], Y Tsui[1], M D Ainslie[1], S Speller[2] and J H Durrell[1]

[1] Department of Engineering, Cambridge University, Trumpington Road, Cambridge CB2 1PZ, United Kingdom
[2] Department of Materials, Oxford University, Banbury Road, Oxford OX2 6HT, United Kingdom
[3] Shanghai Key Laboratory of High Temperature Superconductors, Department of Physics, Shanghai University, Shanghai 200444, People's Republic of China

E-mail: dam72@cam.ac.uk

Received 10 March 2021, revised 10 May 2021
Accepted for publication 8 June 2021
Published 5 July 2021

Abstract

Bulk superconductors can act as trapped-field magnets with the potential to be used for many applications such as portable medical magnet systems and rotating machines. Maximising the trapped field, particularly for practical magnetisation techniques such as pulsed field magnetisation (PFM), still remains a challenge. PFM is a dynamic process in which the magnetic field is driven into a superconducting bulk over milliseconds. This flux motion causes heating and a complex interplay between the magnetic and thermal properties. In this work, the local flux density during PFM in a MgB_2 bulk superconductor has been studied. We find that improving the cooling architecture increases the flux trapping capabilities and alters the flux motion during PFM. These improvements lead to the largest trapped field (0.95 T) for a single MgB_2 bulk sample magnetised by a solenoidal pulsed field magnet. The findings illustrate the fundamental role bulk cooling plays during PFM.

Keywords: pulsed field magnetisation, flux jump, MgB_2 bulk superconductor, trapped-field magnet

(Some figures may appear in colour only in the online journal)

1. Introduction

Trapped-field magnets utilise vortex flux pinning in type-II superconductors to generate large static fields which persist until warming. For many applications, the most practical approach for magnetising such magnets is pulsed field magnetisation (PFM) due to the relatively simple experimental infrastructure [1]. However, the trapped field achievable is less than field cooled magnetisation (FCM) [2, 3]. The trapped field is limited by heat generated during the magnetisation process. This heating simultaneously reduces the critical current density and causes instabilities in the internal magnetic structure leading to lower trapped fields.

Flux jumps are the main thermomagnetic instabilities in PFM and are created by a feedback loop; the penetrating flux generates heat which in turn reduces the local critical current density (j_C) leading to greater flux penetration and therefore further heating [4]. If the decreased $j_C(T)$ cannot be compensated, either by external cooling or by heat distribution through the bulk [5], an uncontrolled surge of flux motion occurs. Therefore, flux jumps are influenced by both the magnetic and thermal properties. To understand the balance between these two factors the dimensionless parameter τ is often considered. τ is the ratio of the magnetic (t_m) and thermal (t_k) time constants:

* Author to whom any correspondence should be addressed.

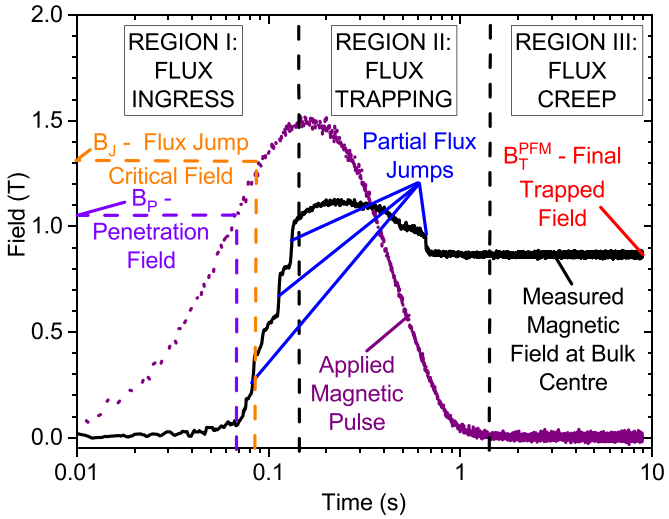

Figure 1. Illustrative data taken from this work (20 K, encapsulated head) displaying the three distinct regions of PFM—(1) rising applied field—flux ingress, (2) declining applied field—flux trapping, and (3) no applied field—flux creep. The flux jump critical field (B_J) is the applied magnetic field when the first flux jump occur. The penetration field (B_P) is the applied field when the magnetic penetrates to the bulk centre.

$$\tau = \frac{t_m}{t_k} = \frac{\mu_0 \kappa}{C \rho_{ff}} \tag{1}$$

where ρ_{ff} is the flux flow resistivity, μ_0 is the permeability of free space and κ is the heat conductivity. For $\tau \ll 1$ ($t_m \ll t_k$), rapid propagation of flux is accompanied by adiabatic heating of the superconductor. Conversely, for $\tau \gg 1$ ($t_m \gg t_k$), the magnetic flux remains fixed during the stage of rapid heating. One way of characterising flux jumps is the first flux jump critical field (B_J)—defined as the applied magnetic field where the first flux jump occurs (figure 1). B_J has been theoretically predicted in various models utilising a range of assumptions [4–8]. Collectively, these models have indicated several parameters which may influence B_J including: critical current density, external cooling capabilities, pulsing temperature, and magnetic field ramp rate. These factors can be vastly different between materials and experimental set-ups making simple comparisons between studies difficult. In MgB_2, the high thermal conductivity and low specific heat leads to a larger temperature rise, under identical heat generation, and faster heat diffusion compared to REBCO bulks. However, the validity of these models during PFM is yet to be established.

Within the existing literature, flux jumps have dominated the discussion on flux motion during PFM [9]. However, in addition to the flux jump driven motion, a variety of other mechanisms are possible depending on the applied field and thermal environment. During PFM, three distinct regions of flux motion are observed, as shown by figure 1. In each region, different mechanisms may drive the flux motion. For regions I (rising applied field) and II (declining applied field), viscous flux flow, flux creep and flux jumps may occur while in Region III (no applied field) the flux motion is limited to flux creep and flux jumps. The interplay between these different types of flux motion is still poorly understood in PFM.

MgB_2 is an intriguing candidate for fabricating trapped-field magnets. While the FCM trapped field is significantly lower than (RE)$Ba_2Cu_3O_{7-\delta}$ (REBCO) based materials (in which the rare earth is one of a number of possibilities—Y, Gd, Nd, Eu, Sm) based bulks (4 T [10] compared to 17.6 T [11]) the processing techniques are uncomplicated and the base materials are both cheaper and less dense. Furthermore, due to the absence of weak-link behaviour, multi-grain samples display strongly connected superconductivity allowing straightforward manufacture of large samples [12–15]. In MgB_2, the PFM approach has been shown to trap significant fields with a maximum of 1.1 T attained in a simple MgB_2 bulk configuration using a split-coil magnet [16]. However, multi-pulse techniques, which have been shown to produce higher trapped fields in REBCO PFM [17], have yet to be systematically conducted in a single bulk MgB_2 sample.

In this paper, we consider the effect of improved sample cooling and repeated pulsing on the trapped field and flux dynamics of a single MgB_2 bulk. A systematic study of the influences on the flux motion and flux jumps is conducted. Furthermore, we present a brief introduction on how remanent magnetisation affects the flux motion behaviour building on existing numerical studies in bulk PFM [18].

2. Experimental details

A single bulk of MgB_2 generated by an *ex-situ* field assisted sintering technique was studied in this work. The bulk has dimensions of 20.5 mm diameter and 3.3 mm thickness. It was chosen for further examination as it demonstrated the highest PFM trapped field from a range of MgB_2 bulks. The bulk was sintered at 1300 °C and 50 MPa for 5 min. Further details of the sintering process can be found in [15]. The absolute trapped field potential of the sample was characterised by FCM utilising a 12 T large bore magnet system with precise control of the bulk temperature. We note that there is not a direct correlation between FCM and PFM trapped field from our range of samples indicating the complex interplay between local superconducting properties, flux motion and the final trapped field.

The principal elements of the PFM experimental apparatus are a Gifford–McMahon cryo-cooler, capacitor bank and control electronics (shown schematically in figure 2). The cryogenic set-up is shown in figure 3. The cryo-cooler conductively cools the sample to a base temperature of 17 K. Throughout the measurement process, the temperature was monitored and controlled using two temperature sensors—one contained within the sample head and another mounted on the bulk surface (see figure 4 for both cooling architectures). The local magnetic flux density was measured using an array of four Hall sensors (Lakeshore HGT-2101) which were calibrated in-house. These were mounted on a bespoke printed circuit board with a separation of 2.5 mm between the Hall sensors. The field profile from the centre to the edge of the sample is recorded throughout the magnetic pulse (see figure 2). The data is collected at a sampling rate of 2 kHz.

To evaluate the effects of the cooling architecture, the sample was magnetised with two different cooling configurations—labelled as the 'simple' and 'encapsulated'

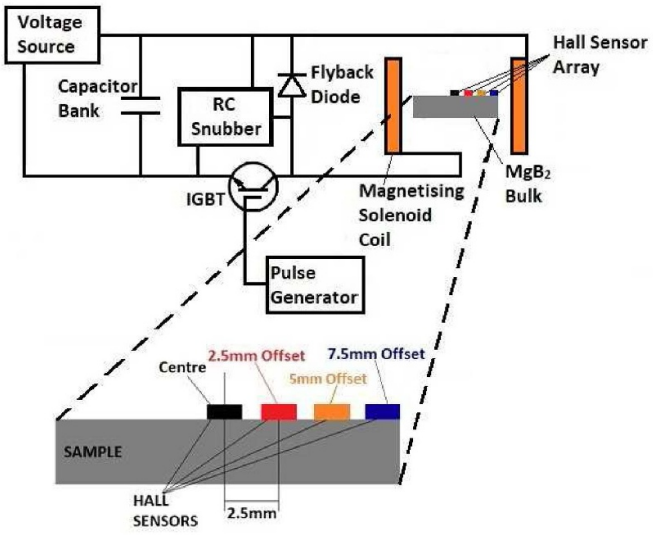

Figure 2. Schematic circuit diagram of the PFM experimental set-up. Expanded schematic view of the Hall sensors distribution and sensor labelling for all experimental set-ups.

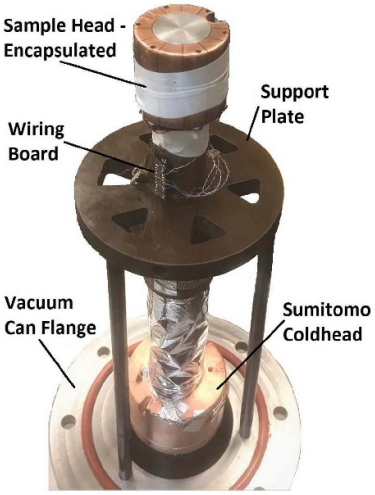

Figure 3. Labelled photograph of cryogenic set-up.

head architectures. In figure 4, the construction of these two heads is shown. For the simple head, the bulk is coated in cryogenic grease (Apiezon N—thermal conductance: $\sim$0.8 W K^{-1} at 20 K [19]) and placed into a bespoke machined copper cup. Therefore, the bulk top surface is exposed and not directly cooled. In contrast, the encapsulated head consists of an additional copper part which surrounds the sample and can clamp the sample to the cold head via indium film. For both heads, the Hall sensor array was positioned on the top surface. However for the encapsulated head the array is embedded into the copper clamp ensuring cooling from all surfaces. In addition, the indium (thermal conductance: $\sim$4 W K^{-1} at 20 K [19]) significantly improves the thermal contact. This improvement was quantified by comparing the temperature variation between the sample head and bulk sample thermometers for a set sample head temperature. At 25 K, we observed a 3 K reduction in the temperature variation in the encapsulated head (29 K for simple head, 26 K for encapsulated head) indicating an improved thermal environment. The encapsulated head is slotted to minimise eddy current generation. We observe no variation in the magnetic pulse response between heads. It should be noted that the pulsing temperature used below is taken from the bulk sample thermometer temperature.

The pulsed magnetic field is created by discharging a capacitor bank through a copper solenoid immersed in liquid nitrogen. This discharge is controlled utilising an insulated gate bipolar transistor (IGBT) which allows rapid switching of the discharge circuit. By altering this switching, the pulse shape can be modified from the standard LCR behaviour to create waveform controlled pulse magnetisation [20, 21]. The magnetic pulse is defined by three user-controlled parameters: the capacitor bank voltage, the switching frequency and the duty cycle:

$$\text{Duty Cycle} = \frac{T_{on}}{T_{on} + T_{off}} \tag{2}$$

where T_{on} and T_{off} are the IGBT open time and off time respectively.

The selected capacitor bank voltage, switching frequency and duty cycle leads to distinct pulses which can be best described by the maximum field, rise time and fall time. The rise time is the time taken to achieve the maximum field and the fall time is the time taken for the generated magnetic pulse to return to zero, see figure 5(a). In this work, a switching frequency of 450 Hz was applied throughout. To illustrate the effect of varying duty cycle at constant capacitor voltage, the generated field normalised to the respective maximum field is displayed in figure 5(b). For this work a 10% duty cycle pulse leading to a rise time of 140 ms will be utilised. We focus on the 10% duty cycle pulses as they lead to the largest trapped fields in the encapsulated head. Two specific pulses will be displayed in this work: initial and optimal. Initial pulses are conducted in the virgin magnetic state after the sample has been stabilised at the pulsing temperature. A pulse leading to the maximum final trapped field is defined as optimal.

3. Results and discussion

3.1. Field cooled magnetisation

To ascertain the trapped field capability of the bulk, the FCM trapped field (B_T^{FC}) was measured. This was achieved by cooling the sample in a static 7 T field from 40 K to the required temperature then ramping the magnetic field to zero at a 0.1 T min^{-1} sweep rate. In figure 6, this downward field sweep is shown at 15 K for three positions along the bulk. The measured field at zero applied field represents B_T^{FC}. This procedure was replicated at 20, 25, 28 and 32 K to generate B_T^{FC}, as shown in the inset of figure 6.

In most experimental studies, the 'local' critical current density (j_C), calculated from small sub-sections of the bulk using magnetisation data [14, 15], is used to characterise the sample performance. However, the large-scale properties are the true measure of sample performance for bulk trapped-field magnets. In large samples, the average, in-field critical current

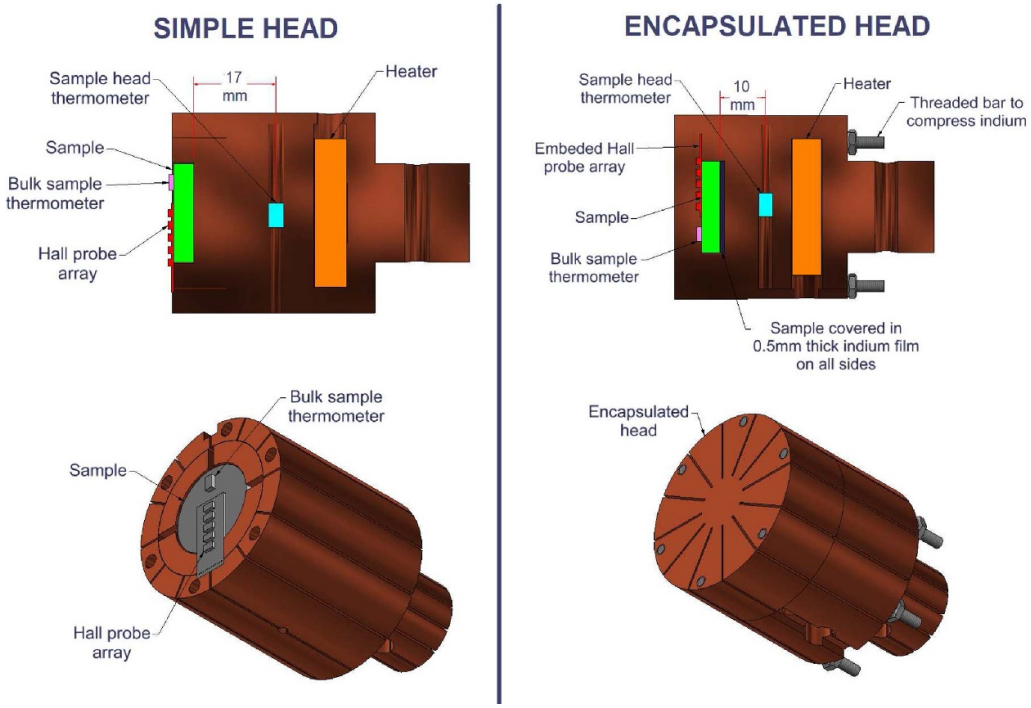

Figure 4. Comparison between simple head and encapsulated head cooling architectures.

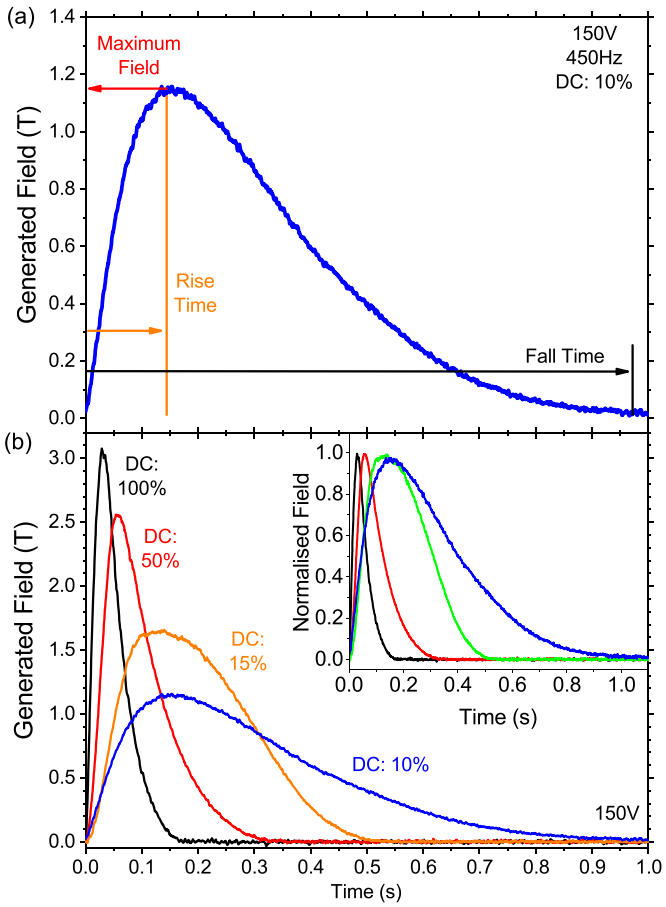

Figure 5. (a) 10% duty cycle generated pulse with 150 V capacitor voltage. The definitions of the rise time and fall time are shown graphically. (b) Representative generated pulses at 150 V with changing duty cycle. Inset: generated field normalised by maximum field for 150 V applied voltage with changing duty cycle.

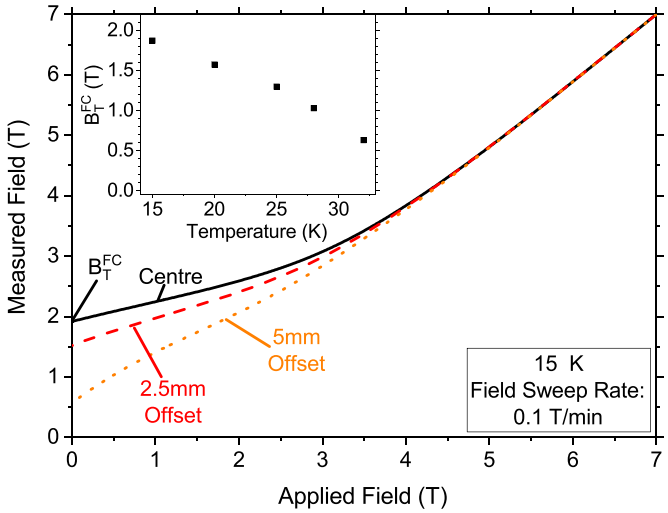

Figure 6. Field-cooled (FC) data of sample at 15 K. Definition of the FC trapped field value (B_T^{FC}) is shown. Inset: B_T^{FC} at all pulsing temperatures.

Table 1. FC trapped field (B_T^{FC}) and bulk critical current density (J_C).

Temperature (K)	B_T^{FC} (T)	J_C ($\times 10^8$ A m^{-2})
15	1.87	4.1
20	1.57	3.5
25	1.29	2.9
28	1.02	2.3
32	0.63	1.4

density (J_C) can be limited by large scale sample inhomogeneities not observed in small sections. Furthermore, the J_C and its temperature dependence is expected to drive the flux jump behaviour.

To derive J_C directly from the FCM trapped fields we follow Fuchs *et al* [10]:

$$J_C = \frac{2B_T^{FC}}{h \ln \frac{1+\sqrt{1+g^2}}{g}} \tag{3}$$

where $g = \frac{h}{R}$, R is bulk radius and h is the bulk thickness. In table 1, the B_T^{FC} and J_C are displayed for reference. We find that the J_C is around an order of magnitude less than j_C (2×10^9 A m^{-2} at 20 K) as derived from vibrating sample magnetometer measurements in a similar bulk with comparable B_T^{FC} cut into small-scale cuboid samples (approximately $2 \times 2 \times 3$ mm).

3.2. Factors influencing final trapped field

In the existing literature, studies optimising the final trapped field in MgB_2 bulk samples have focussed on exploring bulk properties [22, 23] or the use of split-coil magnetic field geometries [24]. The effect of interfacial cooling has not been explicitly explored despite numerical studies indicating its significance during magnetisation experiments [25]. In this

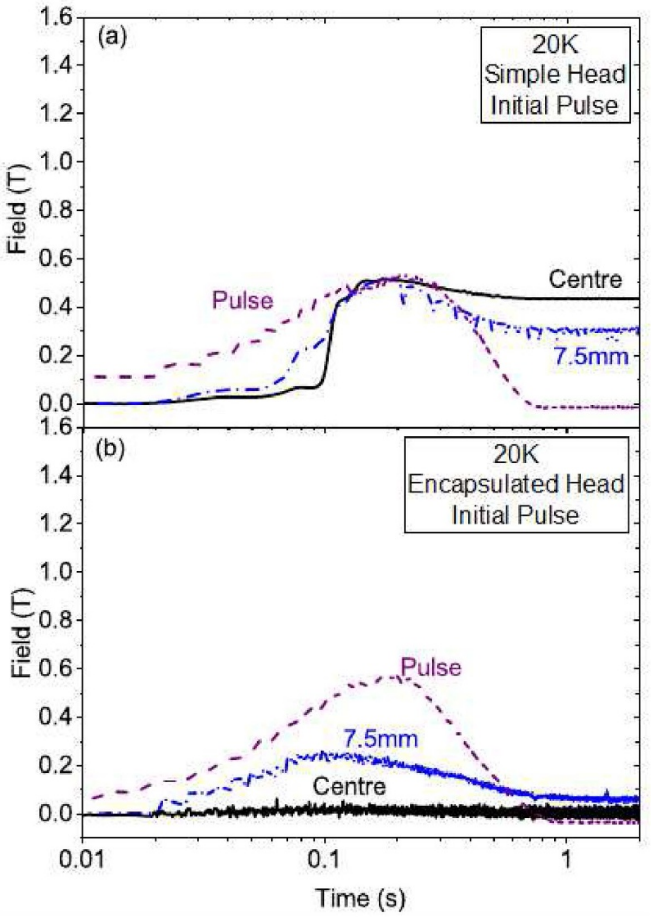

Figure 7. Comparison between flux density variation for initial pulses in simple ((a) maximum field: 0.52 T, RT: 140 ms)) and encapsulated heads ((b) maximum field: 0.62 T) at 20 K.

section, we consider the effects of both improved cooling and iterative multi-pulsing on the final trapped field and flux dynamics.

In figure 7, similar magnitude initial pulses are shown for the simple (a) and encapsulated (b) heads. For the simple head, the measured field rises sharply during flux ingress and becomes equal to the applied field throughout the bulk. This indicates that the induced shielding current, and thus J_C, has reached zero throughout the sample—a full flux jump has occurred. In the encapsulated head, for a comparable applied field we observe no flux penetration to the bulk centre (figure 7(b)). We suggest that the improved cooling has limited the temperature rise at the bulk periphery leading to increased shielding.

If we apply larger magnetic pulses to the encapsulated head, flux can be driven to the bulk centre, as shown in figure 8. For comparison, the behaviour in the simple head is shown in figure 9 A number of features are apparent in this data. For temperatures below 32 K, the penetration is driven by partial flux jumps (where some superconductivity is retained) rather than the full flux jumps observed in the simple head. Furthermore, by measuring the flux profile across the bulk, we observe that partial flux jumps can occur in the outer regions without an observable response at the bulk centre illustrating

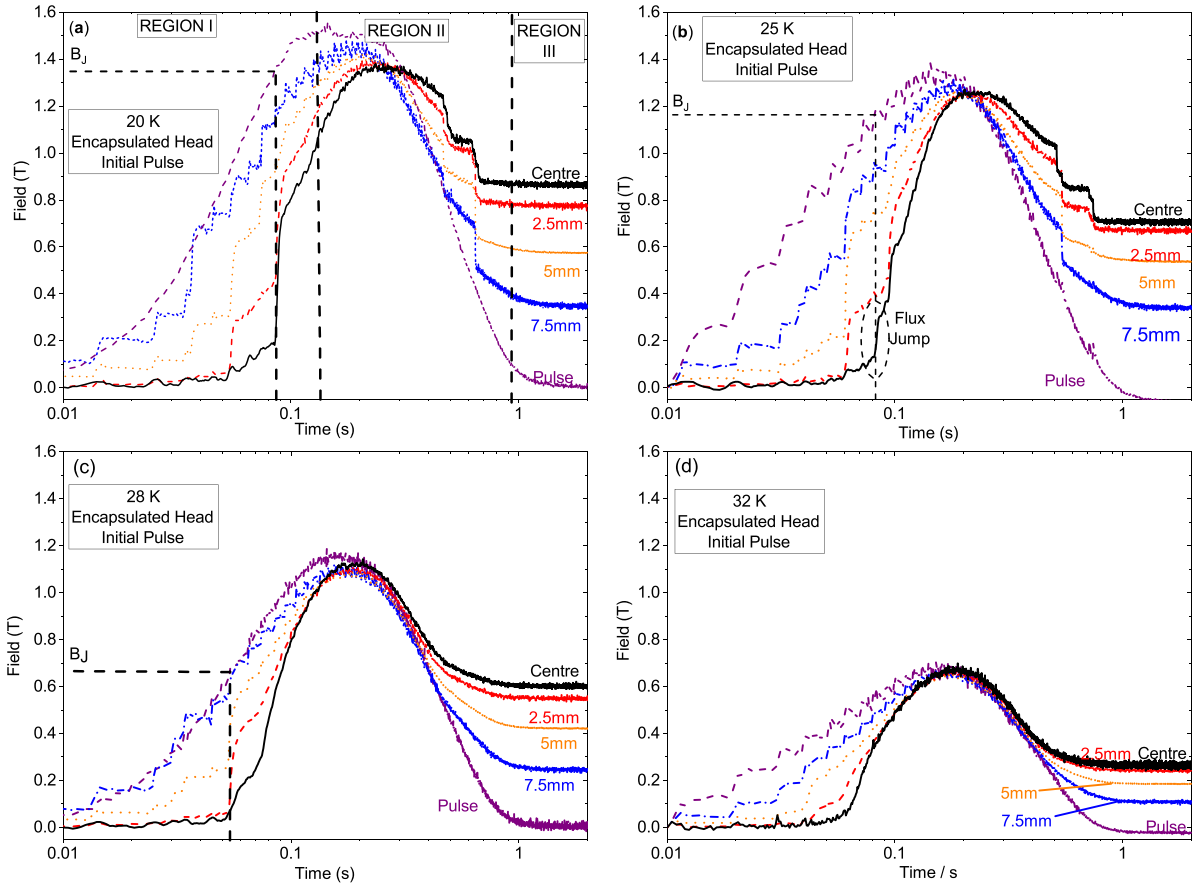

Figure 8. Variation in flux density for initial pulses in encapsulated head ((a) 20 K (maximum field: 1.47 T), (b) 25 K (maximum field: 1.36 T), (c) 28 K (maximum field: 1.17 T), (d) 32 K (maximum field: 0.70 T)).

the importance of Hall sensor array in accurately capturing the flux dynamics. As will be discussed in further detail below, the main limitation in the final trapped field are region II flux jumps leading to rapid flux loss. Unlike the flux penetration, the region II flux jumps occur throughout the bulk and are not restricted to the periphery.

We note that Hirano *et al* [26] have a developed a composite system of soft iron, copper and bulk MgB_2 ring displaying similar improved flux jump stability. Our data further illustrates that interfacial cooling plays the most influential role on PFM flux dynamics.

We now consider the effects of multi-pulsing. In figure 10, the optimal pulses for the encapsulated head are displayed. The maximum trapped field always occurs after a near optimal pulse which lead to a significant remanent field in the bulk. In REBCO bulks it has been shown that a specific multi-pulsing technique leads to the highest trapped field: priming the bulk with an M-shaped remanent field at high temperature then conducting a secondary pulse at a lower temperature [3]. This process can drive preferential flux jumps to the bulk centre [9]. However, we find that the optimum trapped field in MgB_2 occurs with simple iterative pulsing techniques without the requirement for a M-shaped remanent field or varying temperature. We relate this to the negative role played by flux jumps in MgB_2 PFM. Indeed in MgB_2 bulks, the iterative pulsing leads to the flux front uniformly penetrating the sample without flux jumps, as shown in figure 10 [26]. This behaviour is commonly explained by the reduction in heat generated with repeated pulsing [26, 27]. However, the interplay between the remanent magnetisation and penetrating flux is still not well understood. Recent numerical studies in high temperature superconductor (HTS) bulks [28] and stacked tapes [29] have indicated that the flux penetration velocity is reduced during multi-pulse magnetisation. Ascertaining the relative influence of these behaviours and more complex interactions with the remanent magnetisation, as hinted by the M-shaped remanent field techniques, is still an open question. Careful studies of the temperature profile throughout the bulk during PFM may elucidate this issue. However, it is clear that the remanent magnetisation can mitigate region I flux jumps in MgB_2 bulks and appears essential in improving the final trapped field. Note that for greater applied fields than the optimal pulses, region I flux jumps will occur leading to substantial heating and a reduction in the final trapped field.

In contrast to region I flux jumps it is clear that region II flux jumps act solely to reduce the final trapped field. Unfortunately, these flux jumps are accentuated by the nature of PFM—rapid field inversion is inevitable during the magnetisation process. The rapid transition from flux ingress to flux exit can lead to greater heat generated as flux motion occurs during both periods, as shown in figure 10(c). This heating occurs throughout the bulk and can initiate flux jumps, see,

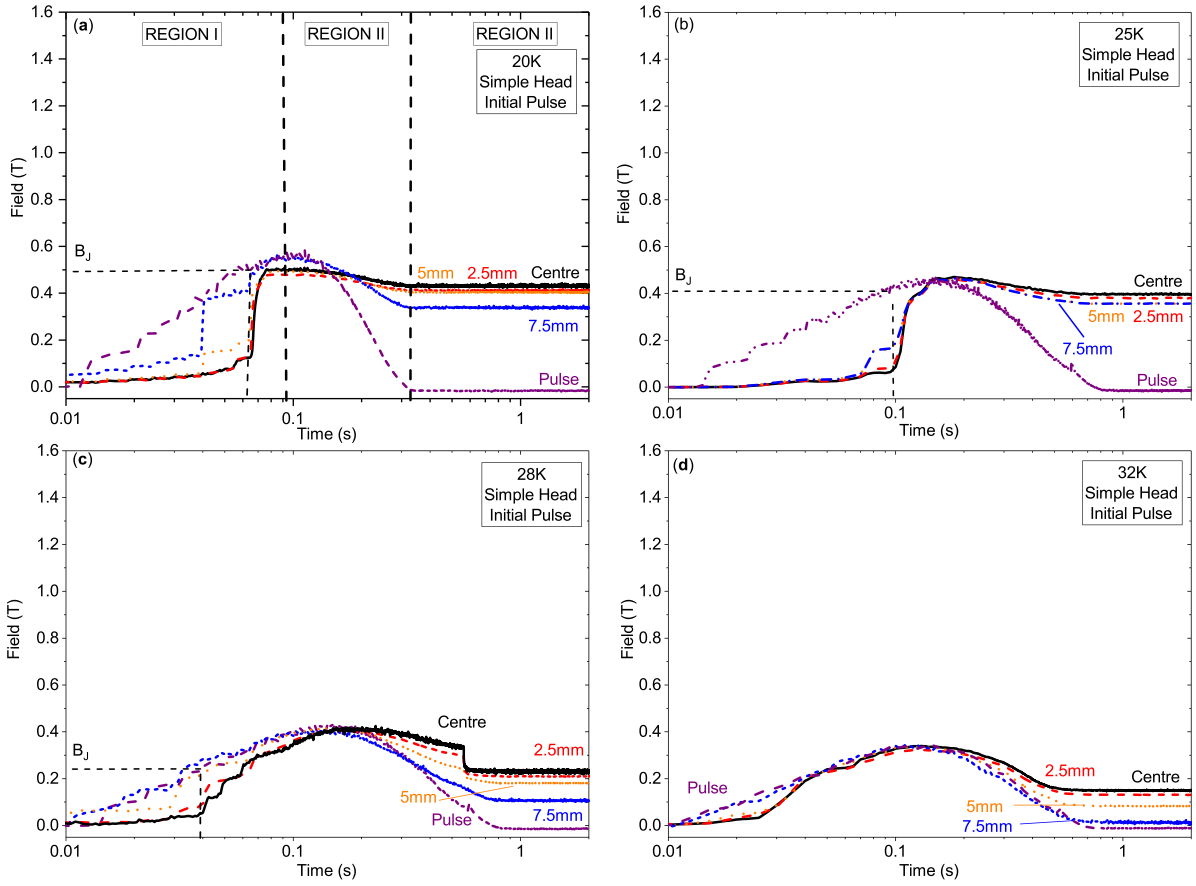

Figure 9. Variation in flux density for initial pulses in simple head ((a) 20 K (maximum field: 0.60 T), (b) 25 K (maximum field: 0.43 T), (c) 28 K (maximum field: 1.17 T), (d) 32 K (maximum field: 0.34 T)).

for example, figure 10(b). Despite the increased cooling in the encapsulated head, this heat generation has not been completely mitigated. However, as in the region I flux jumps, the increased interfacial cooling turns full flux jumps into partial ones improving the final trapped field.

In figure 11, the maximum PFM trapped fields for the encapsulated and simple heads are displayed in comparison to B_T^{FC}. At 20 K, the maximum trapped field in the encapsulated head reaches 0.95 T which is a record for a single MgB_2 bulk. This correlates to an increase of ∼0.45 T in final trapped field at both 20 and 25 K compared to the simple head—a 90% relative improvement. To illustrate the effects of iterative pulsing, the trapped field for equivalent initial pulses to the optimal pulses are shown for the encapsulated head in figure 11. The iterative pulsing only leads to a 10% increase in trapped field for the encapsulated head. The combination of the iterative pulsing and improved cooling enables 80% of the FCM trapped field to be captured at 28 K. 28 K is the minimum temperature where neither region I or II flux jumps occur demonstrating that flux jump mitigation is essential in optimising the trapped field. We note that in the composite ring system of Hirano *et al* [26] they observed a greater improvement with multi-pulsing. In their work, the internal surface of the ring bulk was also cooled further illustrating the essential role cooling plays in MgB_2 PFM.

3.3. Region I flux jumps

The first flux jump field (B_J) during magnetisation is a well explored topic in HTS superconductors both experimentally [30–32] and theoretically [4, 6, 8, 33]. To date, there is little data in MgB_2 samples nor comparison to the existing theoretical framework. We note that the Hall sensors will measure both a time and spatial average of the true magnetic field which may limit the measurement accuracy. However, the observed trapped fields and consistency between measurements indicate that the dynamic accuracy remains acceptable. Using the initial pulse data shown in figure 8, we find flux jumps are inevitable to force flux to the bulk centre in both the simple and encapsulated heads below 32 K. However, as shown in figure 12, the encapsulated head displays an increased stability to flux jumps compared to the simple head. At 20 K, this correlates to an increase in B_J from 0.51 T in the simple head to 1.33 T in the encapsulated head.

We compare the experimental behaviour to two models: standard critical state models [5, 7] ($B_J^{Critical}$) and the flux creep model of Mints [8] (B_J^{Mints}). All models apply the same qualitative arguments—the heat generated by flux motion must be sufficiently counteracted by the heat distribution to ensure that uncontrolled heating does not occur. In the critical state models, the heat generated is proportional to the magnetic field

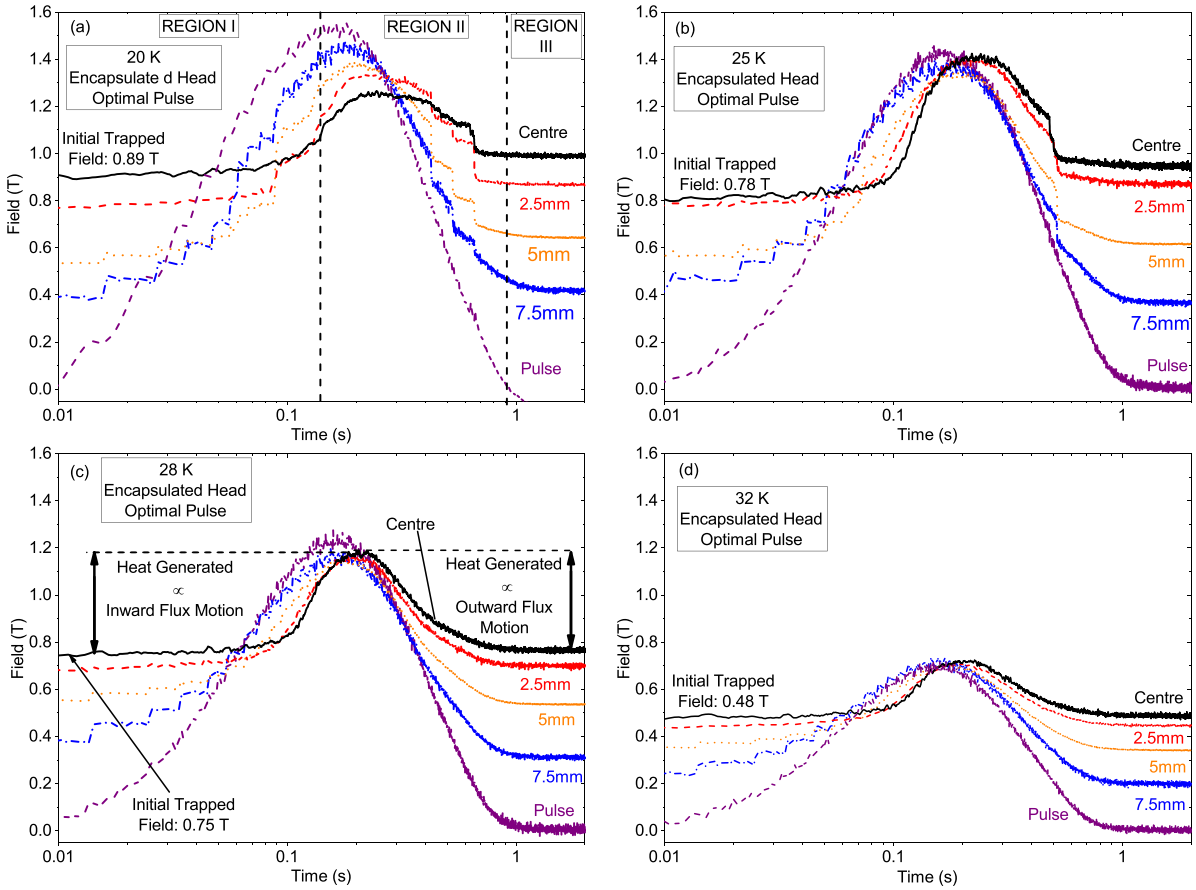

Figure 10. Variation in flux density for optimal pulses in encapsulated head. The optimal pulse occurs as part of an iterative multi-pulse technique ((a) 20 K (maximum field: 1.52 T), (b) 25 K (maximum field: 1.41 T), (c) 28 K (maximum field: 1.23 T), (d) 32 K (maximum field: 0.70 T)).

change [5–7] leading to the same fundamental form in the adiabatic regime ($\tau < 1$):

$$B_J^{Critical} = \left(\frac{\epsilon \mu_0 C J_C}{\left| \frac{\partial J_C}{\partial T} \right|} \right)^{\frac{1}{2}} \tag{4}$$

where ϵ is a numerical factor which varies dependent on the derivation. However, for MgB_2 $\tau > 1$ indicating that the bulk lies within the 'dynamic' regime [34, 35]. Only Akachi *et al* [5] have considered the dynamic regime in the critical state models. By expanding the heat distribution region to the entire bulk, they find that first flux jump field:

$$B_J^{Akachi} = \left[\frac{1}{2} (B_J^{Critical} B_P)^2 \right]^{\frac{1}{4}} \tag{5}$$

where B_P is the penetration field and δ defines the strength of the $J_C(B)$ relationship. To maximise B_J^{Akachi} we assume $\delta = 0$ which is justified by the strong $J_C(B)$ dependence in MgB_2. As the true B_P can be hidden by the flux jump behaviour during the PFM, we have used the B_T^{FC} as a realistic replacement for B_P.

Using the specific heat taken from Wang *et al* [34] and the J_C values derived in section 3.1, we find that B_J^{Akachi} is an order of magnitude smaller than the experimental B_J values. This requires an 'effective' C of 30 000 J m^{-3} K^{-1} which is 75× greater than the internal C at 20 K to match the experimental B_J which cannot be justified physically. In combination with B_J^{Akachi}'s inability to explain the magnetic field ramp rate dependence of B_J often observed in magnetisation studies [30, 31], indicates that the critical state models may not be applicable in PFM.

In contrast to the critical state models, Mints calculates the heat generated from the change in electric field [8]. This enables the integration of the non-linear conductivity of type-II superconductors which can act to stabilise the critical state [36] and generates a magnetic field rate dependence. Within this formulation [8], the first flux jump field for the dynamic regime can be written as:

$$B_J^{Mints} = \left(\frac{2\, h \mu_0^2 J_C^2(T)}{n \left| \frac{\partial J_C}{\partial T} \right| \dot{B}} \right)^{\frac{1}{2}} \tag{6}$$

where T is the sample temperature, h is the heat transfer coefficient on the sample edge and n is the exponent in the $E - J$ power law.

The Mints model is only valid if the bulk is in the flux creep regime during the magnetic pulse. This requires a background

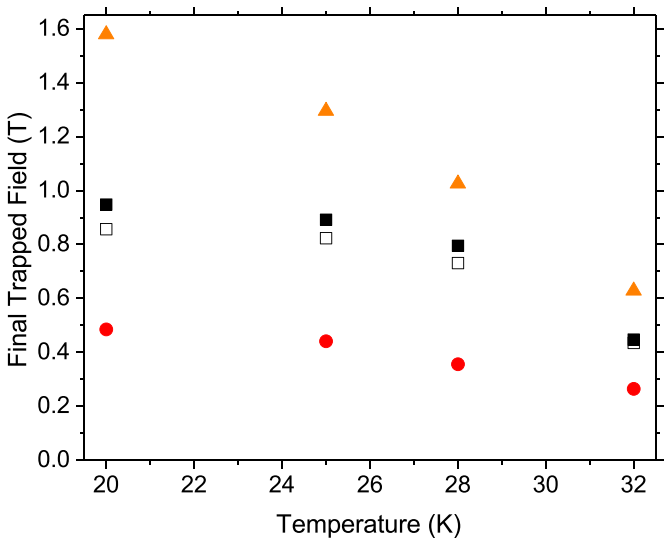

Figure 11. Comparison between the optimal final trapped fields for the encapsulated head (■), simple head (●), and B_T^{FC} at all temperatures (▲). The trapped fields for equivalent initial pulses to the optimal pulses in the encapsulated head are shown with the open symbols (□).

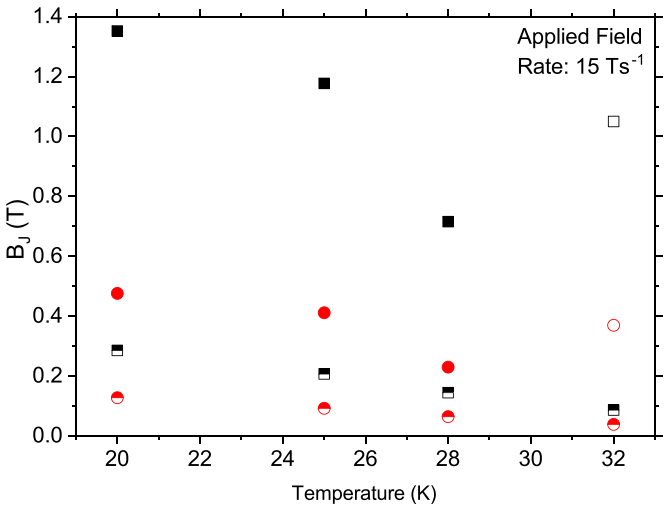

Figure 12. Experimental B_J (encapsulated head—■, simple head—●) compared to the Mints [8] (encapsulated head—◓, simple head—◒, B_J^{Mints}, (6)) critical flux jump field. Open symbols (encapsulated head—□, simple head—○) represent applied pulse fields at 32 K which did not lead to flux jump.

electric field (E_b) below 1 V m^{-1} [25, 37, 38]. To estimate the generated E_b, we apply Maxwell's equations leading to:

$$E_b \sim \frac{B_J \dot{B}}{\mu_0 J_C} \tag{7}$$

where we use the experimental maximum applied field rate ($\dot{B}$—15 T s^{-1}), and the critical state model to estimate the penetration region [8]. From this analysis, background electric fields of around 0.1 V m^{-1} are calculated illustrating that the bulk remains in the flux creep regime. Therefore, it is a common misconception that magnetic pulsing forces the system into the viscous flux flow regime [39, 40]. We have conducted numerical modelling based on the $\boldsymbol{H}$-formulation [41] which generates comparable E_b values.

B_J^{Mints} is sensitive to both the n exponent and the interfacial heat transfer coefficient. There is minimal experimental data for the n exponent in MgB_2 bulks. Therefore, we conducted long-term trapped field measurements on the sample to find n. Our data illustrates that the n exponent is 180 indicating an extremely sharp transition region between the thermally assisted and viscous flux flow regimes. We apply the work of Dillon *et al* [19] to estimate the h values. They found h values of ∼3500 and ∼700 W K^{-1} m^{-2} for indium films and Apiezon-N grease respectively which correspond to the encapsulated and simple heads.

Combining the experimentally derived J_C, $\frac{dJ_C}{dT}$ and n value, B_J^{Mints} is found to be around 6× less than the experimental B_J in both the encapsulated and simple heads, as shown in figure 12. However, the improved stability in the encapsulated head matches the expected $\sqrt{h}$ dependence from B_J^{Mints}. Therefore, further work expanding the Mints model appears justified.

One possible explanation for the magnitude variation in B_J^{Mints} may lie in its theoretical underpinning. To generate a relationship between the temperature and electric field response, Mints equates the decrease in j_C due to sample heating (δj_-) to the increase in current density caused by the flux penetration (δj_+). If the critical state is stable during the pulse then $\delta j_- + \delta j_+ = 0$. However, numerical [18] and experimental [32] studies indicate that the current density can be greater than j_C during the pulse, violating this assumption. Integrating these super-critical j values appears essential in improving the accuracy of B_J^{Mints}. Detailed studies of the induced j or V should help to understand the true nature of the critical state during the magnetic pulse allowing modification of the Mints model. Furthermore, the simple dichotomy between the thermal and magnetic behaviour during PFM seems to be unjustified.

4. Conclusion

PFM flux dynamics in a MgB_2 bulk sample (20.5 mm diameter and 3.3 mm thickness) have been studied for a range of temperatures in two distinct cooling architectures. Through a combination of multi-pulsing and improved cooling architecture, a trapped field of 0.95 T was achieved at 20 K—which we believe is the largest reported PFM value for a single MgB_2 bulk using a solenoid coil. The increased cooling eliminates accumulated heat during PFM improving magnetic shielding and flux jump stability. This leads to a 90% increase in trapped field compared to a simple cup shaped holder. Furthermore, we find the temperature dependence of the first flux jump stability field (B_J). No existing model captures the magnitude of experimental B_J. However, the success of the Mints model in predicting the increased B_J with the improved cooling hints that further theoretical and experimental exploration may prove fruitful. In conclusion, these findings indicate the essential role interfacial cooling plays in determining the final PFM trapped field.

Data availability statement

The data that support the findings of this study are openly available at the following URL/DOI: 10.17863/CAM.65726.

Acknowledgments

This work was supported by the Engineering and Physical Sciences Research Council (Grant Numbers: EP/P023088/1 and EP/P026427/1). Mark Ainslie would like to acknowledge financial support from an Engineering and Physical Sciences Research Council (EPSRC) Early Career Fellowship EP/P020313/1.

ORCID iDs

D A Moseley https://orcid.org/0000-0001-7673-0024
G A B Matthews https://orcid.org/0000-0002-6352-8596
D Zhou https://orcid.org/0000-0001-9889-8872
V Cientanni https://orcid.org/0000-0001-6621-2733
Y Tsui https://orcid.org/0000-0003-1759-0951
M D Ainslie https://orcid.org/0000-0003-0466-3680
S Speller https://orcid.org/0000-0002-6497-5996
J H Durrell https://orcid.org/0000-0003-0712-3102

References

[1] Ikuta H, Ishihara H, Hosokawa T, Yanagi Y, Itoh Y, Yoshikawa M, Oka T and Mizutani U 2000 *Supercond. Sci. Technol.* **13** 846–9
[2] Fujishiro H, Tateiwa T, Fujiwara A, Oka T and Hayashi H 2006 *Physica* C **445–448** 334–8
[3] Fujishiro H, Hiyama T, Tateiwa T, Yanagi Y and Oka T 2007 *Physica* C **463–465** 394–7
[4] Wipf S L 1967 *Phys. Rev.* **161** 404–16
[5] Akachi T, Ogasawara T and Yasukōchi K 1981 *Japan. J. Appl. Phys.* **20** 1559–71
[6] Swartz P S and Bean C P 1968 *J. Appl. Phys.* **39** 4991–8
[7] Müller K H and Andrikidis C 1994 *Phys. Rev.* B **49** 1294–307
[8] Mints R G 1996 *Phys. Rev.* B **53** 12311–17
[9] Zhou D *et al* 2018 *Supercond. Sci. Technol.* **31** 105005
[10] Fuchs G, Häßler W, Nenkov K, Scheiter J, Perner O, Handstein A, Kanai T, Schultz L and Holzapfel B 2013 *Supercond. Sci. Technol.* **26** 122002
[11] Durrell J H *et al* 2014 *Supercond. Sci. Technol.* **27** 082001
[12] Bhagurkar A G, Yamamoto A, Anguilano L, Dennis A R, Durrell J H, Hari Babu N and Cardwell D A 2016 *Supercond. Sci. Technol.* **29** 035008
[13] Gozzelino L *et al* 2019 *Supercond. Sci. Technol.* **32** 034004
[14] Matthews G A B, Liu J, Grovenor C R M, Grant P S and Speller S 2020 *Supercond. Sci. Technol.* **33** 034006
[15] Matthews G A B, Santra S, Ma R, Grovenor C R M, Grant P S and Speller S C 2020 *Supercond. Sci. Technol.* **33** 054003
[16] Fujishiro H, Mochizuki H, Naito T, Ainslie M D and Giunchi G 2016 *Supercond. Sci. Technol.* **29** 034006
[17] Ikuta H, Ishihara H, Yanagi Y, Itoh Y and Mizutani U 2002 *Supercond. Sci. Technol.* **15** 606–12
[18] Ainslie M D, Srpcic J, Zhou D, Fujishiro H, Takahashi K, Cardwell D A and Durrell J H 2018 *IEEE Trans. Appl. Supercond.* **28** 6800207
[19] Dillon A, McCusker K, Van Dyke J, Isler B and Christiansen M 2017 *IOP Conf. Ser.: Mater. Sci. Eng.* **278** 012054
[20] Ida T *et al* 2006 *J. Phys.: Conf. Ser.* **43** 539–42
[21] Ida T, Li Z, Miki M, Watasaki M and Izumi M 2018 *IEEE Trans. Appl. Supercond.* **28** 6801905
[22] Miyazaki T *et al* 2017 *IEEE Trans. Appl. Supercond.* **27** 6800504
[23] Oka T *et al* 2019 *IEEE Trans. Appl. Supercond.* **29** 6802606
[24] Fujishiro H, Mochizuki H, Ainslie M D and Naito T 2016 *Supercond. Sci. Technol.* **29** 084001
[25] Xia J, Li M and Zhou Y 2017 *Supercond. Sci. Technol.* **30** 075004
[26] Hirano T, Takahashi Y, Namba S, Naito T and Fujishiro H 2020 *Supercond. Sci. Technol.* **33** 085002
[27] Fujishiro H, Kaneyama M, Tateiwa T and Oka T 2005 *Japan. J. Appl. Phys.* **44** L1221–4
[28] Ainslie M D, Bumby C W, Jiang Z, Toyomoto R and Amemiya N 2018 *Supercond. Sci. Technol.* **31** 074003
[29] Zou S, Zermeño VM, Baskys A, Patel A, Grilli F, Glowacki BA 2017 Simulation and experiments of stacks of high temperature superconducting coated conductors magnetized by pulsed field magnetization with multi-pulse technique *Supercond. Sci. Technol.* **30** 014010
[30] Gerber A, Li J N, Tarnawski Z, Franse J J M and Menovsky A A 1993 *Phys. Rev.* B **47** 6047–53
[31] Wenger C, Gladun A, Krabbes G and Fuchs G 2001 *IEEE Trans. Appl. Supercond.* **11** 3533–6
[32] Nabiałek A, Vasiliev S, Chabanenko V, Yao X, Cai Y, Guo L and Kuzovui M 2012 *Acta Phys. Pol.* A **121** 836–40
[33] Mints R G and Rakhmanov A L 1981 *Rev. Mod. Phys.* **53** 551–92
[34] Wang Y, Plackowski T and Junod A 2001 *Physica* C **355** 179–93
[35] Sologubenko A V, Jun J, Kazakov S M, Karpinski J and Ott H R 2002 *Phys. Rev.* B **66** 014504
[36] Mints R G and Rakhmanov A L 1982 *J. Phys. D.: Appl. Phys.* **15** 2297–306
[37] Duron J, Grilli F, Dutoit B and Stavrev S 2004 *Physica* C **401** 231–5
[38] Ainslie M D, Zhou D, Fujishiro H, Takahashi K, Shi Y H and Durrell J H 2016 *Supercond. Sci. Technol.* **29** 124004
[39] Itoh Y and Mizutani U 1996 *Japan. J. Appl. Phys.* **35** 2114–25
[40] Mizutani U, Oka T, Itoh Y, Yanagi Y, Yoshikawa M and Ikuta H 1998 *Appl. Supercond.* **6** 235–46
[41] Ainslie M D and Fujishiro H 2015 *Supercond. Sci. Technol.* **28** 053002